



# Investigation and identification of damage mechanisms of unidirectional carbon/flax hybrid composites using acoustic emission

Mariem Ben Ameer, Abderrahim El Mahi, Jean-Luc Rebiere, Isabelle Gimenez, Moez Beyaoui, Moez Abdennadher, Mohamed Haddar

## ► To cite this version:

Mariem Ben Ameer, Abderrahim El Mahi, Jean-Luc Rebiere, Isabelle Gimenez, Moez Beyaoui, et al.. Investigation and identification of damage mechanisms of unidirectional carbon/flax hybrid composites using acoustic emission. Engineering Fracture Mechanics, 2019, 216, pp.106511. 10.1016/j.engfracmech.2019.106511 . hal-02954698

**HAL Id: hal-02954698**

**<https://hal.science/hal-02954698>**

Submitted on 25 Oct 2021

**HAL** is a multi-disciplinary open access archive for the deposit and dissemination of scientific research documents, whether they are published or not. The documents may come from teaching and research institutions in France or abroad, or from public or private research centers.

L'archive ouverte pluridisciplinaire **HAL**, est destinée au dépôt et à la diffusion de documents scientifiques de niveau recherche, publiés ou non, émanant des établissements d'enseignement et de recherche français ou étrangers, des laboratoires publics ou privés.



Distributed under a Creative Commons Attribution - NonCommercial 4.0 International License

# **Investigation and identification of damage mechanisms of unidirectional carbon/flax hybrid composites using acoustic emission.**

Mariam Ben Ameer<sup>1,2</sup>, Abderrahim El Mahi<sup>1</sup>, Jean-Luc Rebiere<sup>1</sup>, Isabelle Gimenez<sup>3</sup>, Moez Beyaoui<sup>2</sup>, Moez Abdennadher<sup>2</sup>, Mohamed Haddar<sup>2</sup>

<sup>1</sup> Acoustics Laboratory of Le Mans University (LAUM) UMR CNRS 6613, Av. O. Messiaen, 72085, Le Mans cedex 9, France.

<sup>2</sup> Laboratory of Mechanics, Modeling and Production (LA2MP), National School of Engineers of Sfax, University of Sfax, BP N° 1173 - 3038, Sfax, Tunisia

<sup>3</sup> Le Mans Technology Transfer Center (CTTM), 20 rue Thalès de Milet, 72000 Le Mans, France.

Corresponding author: Mariem.Ben\_Ameer.Etu@univ-lemans.fr (M. Ben Ameer)

## **Abstract**

The objective of the present experimental work is to determine the damage mechanisms appearing in unidirectional carbon/flax hybrid composites during tensile tests. The specimens tested consist of unidirectional carbon and flax fiber plies with different stacking sequences. Laminated composites were manufactured using a manual lay-up process. The specimens were tested under uniaxial tensile loading in static and cyclic fatigue tests. The tests carried out were monitored by the acoustic emission (AE) technique in order to identify the damage mechanisms evolutions. This identification was made with an unsupervised clustering technique. The recorded events were classified with the k-means algorithm based on temporal classification parameters. For each kind of specimen, four classes of AE events were obtained. Then, the contribution of each damage mechanism to overall failure was evaluated by the amplitude range, the cumulative number of hits and the acoustic energy activity. The AE classes obtained were correlated with scanning electron microscopy (SEM) observations in order to identify the damage mechanisms observed.

## **Keywords**

Carbon fibers; flax fibers; hybrid composites; acoustic emission; damage mechanisms.

## 1. Introduction

Natural fibers such as flax, sisal and hemp have great advantages, in comparison with synthetic fibers, that make them interesting and competitive materials for composite structure applications. The use of polymer with agro-based fibers has been the subject of many research works due to the awareness of researchers to the environmental challenges. For instance, their availability, their ecological aspect and their biodegradability are some factors for reducing the environmental impact [1, 2]. Also, they are characterized by their low costs. More especially, they present a potential alternative to conventional fibers owing to their specific properties. In fact, agro-based fibers exhibit a stiffness comparable to those of glass fibers. Moreover, they are about 50% lighter than glass ones [3, 4]. The use of flax fibers as reinforcement of polymer matrix composites has been of particular interest to many researchers. Flax fibers are used in different forms (short fibers, monofilaments, unidirectional flax tape, woven fabrics, etc...) for reinforcing polymer matrix (thermoplastic or thermoset resin) with different types of manufacturing processes (stacking sequence, vacuum bag molding process, liquid resin infusion, resin transfer molding, etc...) [5 - 9]. Monti et al. [10] studied the damping properties of unidirectional flax fiber reinforced composites. Yan et al. [11], Monti et al. [12] and Haggui et al. [13] evaluated the mechanical properties of unidirectional flax polymers.

Duc et al. [14] carried out an experimental study to evaluate the mechanical and damping properties of polymer reinforced with carbon, glass and flax fibers. The results revealed that flax fiber laminates present good damping properties but they present lower mechanical properties than carbon and glass fiber laminates. In order to enhance the mechanical performance of agro-based composites, hybridization of flax fibers with carbon ones in the same matrix was proposed [15]. Therefore, hybridization offers to the composite structures' lightness, good damping properties and sufficient mechanical performance. Consequently, they can be suitable for structural use. In addition, by hybridization with carbon fibers, the property of variability and moisture sensitivity of flax fibers can be reduced [16, 17]. The hybrid composites have been recently exploited in industrial applications such as manufacturing tennis rackets (Artengo) and bicycles (Museum bikes). Ben Ameer et al. [18] studied the damping properties of unidirectional carbon-flax hybrid fiber reinforced composites. Flynn et al. [19] analyzed the mechanical behavior of hybridized carbon-flax fiber composites. These hybrid composite structures may have different damage mechanisms which occur when they are subjected to service loading.

In the field of structural health monitoring (SHM), several studies used the electrical resistance variation to assess and monitor the internal damage [20-23]. A breakdown of percolation network, formed by the contacting fibers, results in an increase in electrical resistance. So that, the variation in electrical resistance reflects the damage during the loading process. Other several works used a numerical approach based on the lattice

simulation and the Acoustic Emission (AE) technique [24, 25]. Therefore, they analyzed and verified the relationships between the numerical simulations and the parameters of the AE monitoring. Mostly, the AE technique has been frequently used by different research work to monitor in real time the spread of damage in composite structures subjected to different loading types [26]. It is important to note that this technique is the most advanced method for the non-destructive evaluation of damage progression. AE associated with microscopic analyses can be an effective method to investigate damage mechanisms in composites. In this context, the clustering effect was studied in order to know which damages (matrix cracking, fiber–matrix interface debonding, delamination, fiber pull-out and fiber breakage defects) occurred in the laminates. The use of such method needs a fair understanding of the relationships between the damage process and the recorded signal. Different AE signal analysis methods were utilized in research, such as frequency band, AE counts, amplitude ranges, AE energy or a combination of several AE parameters.

Different damage mechanisms have been identified for flax fiber reinforced composites in several works [12, 13, 27, 28, 29, 30]. According to the work of Bravo et al. [30], the AE events can be classified by their amplitudes. Different amplitude ranges of AE events are attributed to matrix cracking (from 35-42 dB to 45-60 dB). The amplitudes from 45-60 dB to 60-70 dB are assigned to fiber-matrix debonding. The amplitudes of delamination are between 50 dB and 80 dB. The amplitudes between 60 dB and 100 dB are usually attributed to fiber pull-out and fiber breakage. Depending on the type of matrix and fibers used, the ranges of these intervals can change.

Some works focus on the classification of damage mechanisms in laminated carbon/epoxy composites using the obtained frequency results [31,32]. Otherwise, the wavelet transform analysis in the frequency domain can provide more information about the level of damage in composite materials [33-36]. In several works [37-39], the Continuous Wavelet Transform (CWT) was used in frequency domain analysis of the acoustic signals during mechanical testing for detecting and identifying damage mechanisms in carbon fiber reinforced polymers CFRP. The Discrete Wavelet Transform (DWT) has been used by Gutkin et al. in [40] to identify AE signals based on the frequency range and to interpret the types of damage of CFRP laminates. From AE signals recorded during tensile tests on specimens with various layups and orientations, five failure modes are clearly identified; matrix cracking, fiber/matrix debonding, delamination, fiber pull-out and fiber fracture. Barile et al [41] have reported in their work on analyzing the effect of thickness of the material and its geometry in the amplitude and the acoustic energy of the AE signals. Bussiba et al. [42] classified the damage mechanisms of C/C composites during cyclic tests with the acoustic emission technique. They tracked the damage evolution through the AE count rates and cumulative AE counts. They found three active mechanisms of failure: matrix cracking, debonding and fiber fracture. Bouchak et al. [43] tested carbon fiber reinforced plastic composites under static

and fatigue loading with monitoring of damages by AE. They found that AE energy provides a valid and useful damage parameter and effective failure criteria for fatigue life prediction.

For hybrid laminates, Fotouhi et al. [44] investigated the damage modes occurring in thin-ply UD carbon-glass hybrid laminates using acoustic emission. They used a criterion based on amplitude and energy of the AE event values. Saidane et al. [45] tested flax-glass fiber hybrid composites in order to assess the damage mechanisms occurring during tensile tests. Their results showed that all studied laminates present three classes of AE signal (matrix cracking, debonding and fiber breakage). Several research works found that the conventional mono-parametric AE signal analysis may be insufficient and limited in terms of damage identification. This is why, multiparameter statistical analyses have already been used in order to better discriminate and identify the damage modes.

This paper deals with relatively new materials: carbon-flax hybrid composites made of an epoxy matrix reinforced by unidirectional flax and carbon fibers with different content and different lay-up configurations. The damage mechanisms of this type of materials have not been deeply studied yet. The main objective of this study is to identify the failure mechanisms occurring under service loading for the flax fiber laminates, carbon fiber laminates and carbon-flax hybrid laminates. AE damage analysis presented is based on the results of static and fatigue tensile testing. This identification is made using an unsupervised classification with a multivariable statistical technique, based on a pattern recognition method. In fact, the recorded events are classified with the k-means algorithm. By using AE amplitude, vector of hits and contribution of AE energy, the damage mechanisms are classified. Post-test microscopy is performed on failed specimens. The observed damage mechanisms are correlated with the AE classification. Finally, it is found that the used AE technique is an effective method for accurate detection of failure mechanisms, whether in non-hybrid flax and carbon laminates or in carbon-flax hybrid laminates.

## **2. Materials and manufacturing**

The composite materials studied in this work are reinforced with unidirectional flax tape and unidirectional carbon fabric, and a liquid thermoset epoxy resin. The flax tape, provided by the LINEO Company, has an areal density of 200 g/m<sup>2</sup> [46]. The carbon fabric, provided by the SICOMIN Company, has an areal density of 300 g/m<sup>2</sup>. The thermoset epoxy resin used for the composite materials is the SR 1500 epoxy resin mixed with SD 2505 hardener provided by SICOMIN.

First, the fibers were cut from the roller. Flax fibers were dried in an oven for 1 hour at 110°C to remove water and to enhance the mechanical properties [47] but carbon fibers were used as received. After that, carbon and

flax layers were impregnated in the desired stacking sequence using a manual lay-up method with the resin at room temperature (20°C). Then, non-hybrid and hybrid composites were elaborated using a vacuum bag molding process. They were cured at 50 kPa depression and room temperature for 7 hours. There are six stacking sequences with unidirectional laminated plates (non-hybrid:  $[F_3]_s$  and  $[C_3]_s$ , and hybrid:  $[C_2/F]_s$ ,  $[C/F_2]_s$ ,  $[F/C_2]_s$  and  $[F_2/C]_s$ ), as presented in Fig. 1, consisting of 6 layers with fibers in 0° orientation plies. Finally, specimens were cut from the laminated plates with nominal dimensions of 200 mm x 15 mm x h where h is the thickness. The thickness h, fiber volume fraction  $V_f$  and density of different stacking sequence are given Table 1.

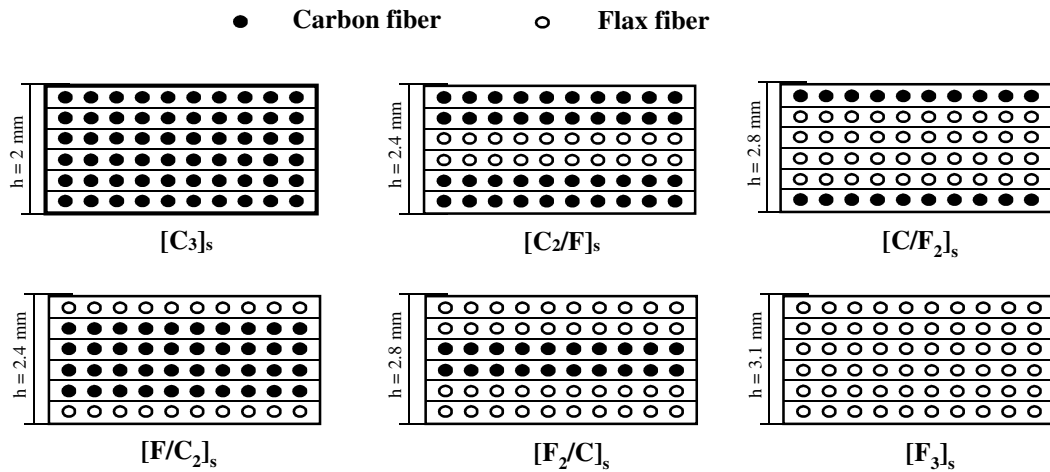


**Fig. 1.** Different stacking sequences of composite laminates with six plies.

**Table 1**

Thickness, fiber volume fraction and density of non-hybrid and hybrid laminates.

Laminates	Nominal thickness h (mm)	Fibre volume fraction $V_f$ (flax/carbon)	Density (Kg/m <sup>3</sup> )
$[F_3]_s$	3.10	0.32/0.00	1140
$[F_2/C]_s$	2.80	0.22/0.19	1181
$[F/C_2]_s$	2.40	0.12/0.37	1266
$[C/F_2]_s$	2.80	0.22/0.19	1175
$[C_2/F]_s$	2.40	0.12/0.37	1234
$[C_3]_s$	2.00	0.00/0.55	1340

### 3. Experimental setup

Static and fatigue tensile tests were performed on non-hybrid and hybrid laminates until failure. They were carried out on a servo-hydraulic machine INSTRON-8516 equipped with a 100 kN load cell (Fig. 2). The tensile test machine was interfaced with an acquisition system for monitoring and data acquisition. The specimens were tested according to the standard test method ASTM D3039/D3039 M [48]. Three to four specimens were tested for each configuration sample in order to check the reproducibility. For the static tests, specimens were loaded with a displacement rate of 1 mm/min at room temperature.

For the fatigue tests, specimens were tested under load amplitude control. The tests were performed using a sinusoidal type of waveform with a frequency of 10Hz. The applied load ratio used was equal to  $R_F = F_{min}/F_{max} = 0.1$  and the applied load level used was equal to  $r_F = F_{max}/F_u = 0.75$ , where  $F_{min}$ ,  $F_{max}$  and  $F_u$  are respectively, the minimum applied load, the maximum applied load and the ultimate failure load determined from the static tests.

During the static and fatigue tensile tests, damage and fracture progression in the tested specimens were analyzed by the AE method. Two resonant piezoelectric sensors (PCA MICRO-80) with a frequency bandwidth of 100 kHz-1 MHz and a resonance peak of 300 kHz, provided by Euro Physical Acoustics (EPA) corporation, were used. They were clamped to the specimens on the same side with a plier using a coupling agent (silicon grease) between the specimen and the sensors. For best results, we do not take too much of the coupling agent. Therefore, a thin layer of grease was used on the sensor against the specimen surface. These AE sensors were used to record the transient waves propagated through the material under loading. These acoustic waves were generated as a consequence of elastic deformations and damage mechanisms. In fact, events created in the gauge length and under grips were recorded. The gauge length was 100 mm. In the interest of reducing the attenuation of the waves originating from the source, the distance between the two AE sensors was set to 50 mm. The recorded AE signals were amplified and filtered using two pre-amplifiers with a gain of 40 dB, provided by Mistras Group Company. The acquisition of the acoustic emission signals was processed using the AEwin software, provided by EPA corporation, with a sampling frequency rate of 5 MHz. This system was equipped with a PCI acquisition card connected to the micro-computer (Fig. 3). The AE data were dependent on temporal acquisition parameters, namely: PDT (Peak Definition Time), HDT (Hit Definition Time) and HLT (Hit Lockout Time) [30]. The values of these temporal parameters were set to: PDT = 50  $\mu$ s, HDT = 100  $\mu$ s and HLT = 200  $\mu$ s. The amplitude of the acquisition threshold was determined using the Pencil Lead Breaking (PLB) procedure [49, 50] and was equal to 40 dB in order to filter the AE signals coming from external sources (noise). For each

stacking sequence fractured in the tensile test, macroscopic and microscopic observations and analyses of the failure mode were carried out. Samples extracted from the specimens tested under tensile loading were prepared. For the macroscopic analysis, visual inspection was done to identify damage mechanisms in the broken specimens such as delamination or fiber pull-outs. For the microscopic analysis, scanning electron microscopy (SEM) was used to detect smaller damage mechanisms of failure profiles.

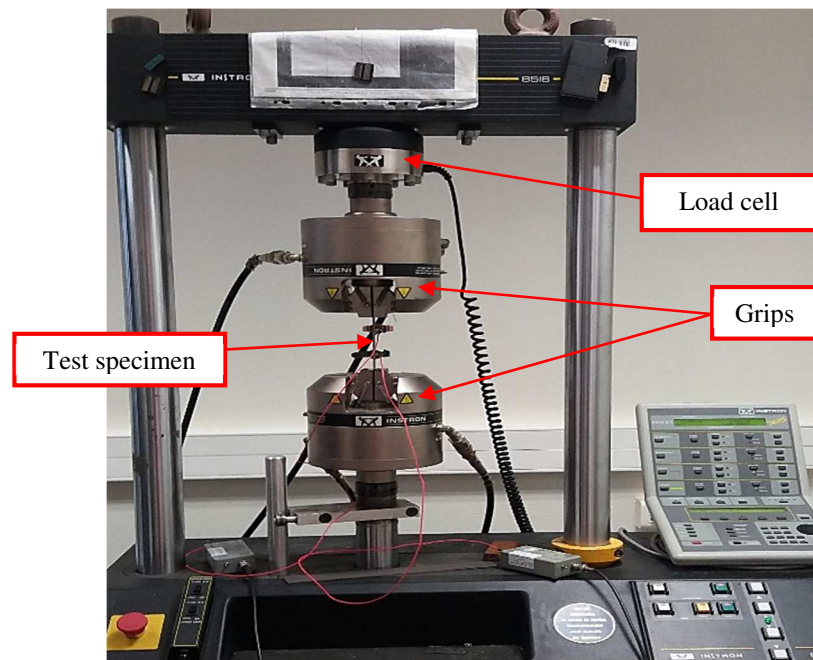


**Fig. 2.** Experimental setup of tensile test.



**Fig. 3.** Experimental setup of acoustic emission method.

## 4. Results and discussion

### 4.1. AE data classification

The AE method of classification was used to identify the damage mechanisms for the detected AE signals. The AE data sets were processed using NOESIS software [51]. Five temporal parameters were selected for the



classification of the acoustic emission signals: amplitude, rise time, duration, number of counts to peak and energy. They are explained below and illustrated in Fig. 4.

- Threshold: is a level set to distinguish signal from noise.
- Amplitude: is the peak value reached by the signal in an AE event which covers the range from 40 dB to 100 dB
- Rise time: is the time required for the signal to reach the amplitude after crossing the threshold.
- Duration: is the time difference between the first and last threshold crossings with the event signal.
- Number of counts to peak: is the number of times the signal crosses the threshold between the peak amplitude and the threshold.
- Energy: is the area under the curve of amplitude vs time for an event.

The amplitude of the signal was measured by the data acquisition system in real time. The other parameters were calculated by the waveforms recorded using the acquisition system. After several initial trials, these parameters settled, allowing a good repeatability for data classification.

The AE signals were classified by the K-means algorithm [52]. This algorithm is unsupervised pattern recognition analysis. It aims to split a set of  $n$  events into an optimal number of  $k$  clusters in which the sum of squared distances between all the vectors of a class and its center is minimized. The normalization of the descriptors of the vector representative of an acoustic emission signal is indispensable. The difference in scale of the different parameters can lead to one parameter hiding the others because of its important values. The data sets were normalized by the following transformation:

$$\forall i \in \Omega_p, p \in F : z_i = \frac{x_i - m_{x_p}}{\sigma_{x_p}}. \quad (1)$$

where  $x_i$  is the event  $i$  of a set of data  $\Omega_p$  related to the acoustic feature  $p$ ,  $m_{x_p}$  and  $\sigma_{x_p}$  are respectively the average value and the standard deviation of  $\Omega_p$ , and  $F$  the set of features chosen for the classification. The k-mean algorithm was used with Euclidian norm and random initial partitioning.

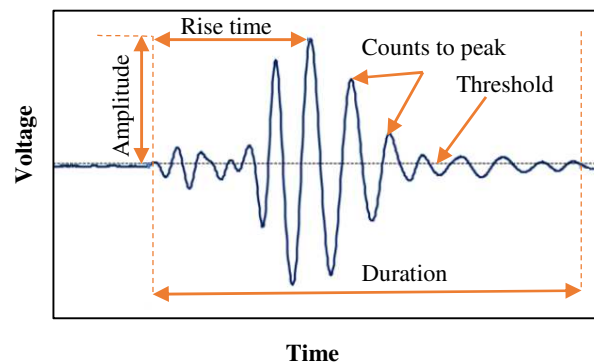


**Fig. 4.** Typical acoustic emission waveform and its parameters.

## **4.2. Acoustic emission under static tensile tests**

### **4.2.1. Investigation of the damage evolution by monitoring the AE activity**

The acoustic activity is presented by the evolution of the cumulative number of vector of hits. Fig. 5 presents the correlation between the evolution of the acoustic activity and loading data versus strain within the specimen. An exponential type of curve is obtained for the AE response. It can be noticed from Fig. 5 that the acoustic activity and the evolution of the loading take place in three phases [53]:

-Phase I: First linear elastic phase characterized by very few detections of AE activity. It seems to be a silent period. In this phase, no damage is initiated. In fact, this loading not having any effect on the specimen's integrity.

-Phase II: Here the stress curve begins to lose its linearity slightly. Its slope decreases, reflecting the onset of viscoelastic behavior. This phase is characterized by a steady increase in acoustic activity. At first, some events are detected. These events reflect the beginning of micro-cracks in the resin. Then, the small increase may reflect the onset of fiber-matrix debonding and the micro-cracks evolve and join together to form the delamination.

-Phase III: Finally, the third phase which is just before the specimen's final failure. The stress curve is non-linear, reflecting the beginning of plasticity. AE activity becomes greater. Its curve evolution changes and exhibits a linear form until the specimen's final breakage. An assumption can be made that a new damage mechanism has occurred which is fiber breakage.

In addition, it can be noted from the comparison between all these non-hybrid and hybrid specimens that when the carbon fiber volume fraction increases the cumulative number of counts increases. For instance, the acoustic activity reaches a maximum value of 80000 counts for  $[C_3]_s$  specimen, followed by 34000 and 30000 counts ( $[C_2/F]_s$  and  $[F/C_2]_s$  specimens, respectively) and 12000 and 21000 counts ( $[C/F_2]_s$  and  $[F_2/C]_s$  specimens, respectively). The minimum acoustic activity is observed near 2500 counts in  $[F_3]_s$  specimen.

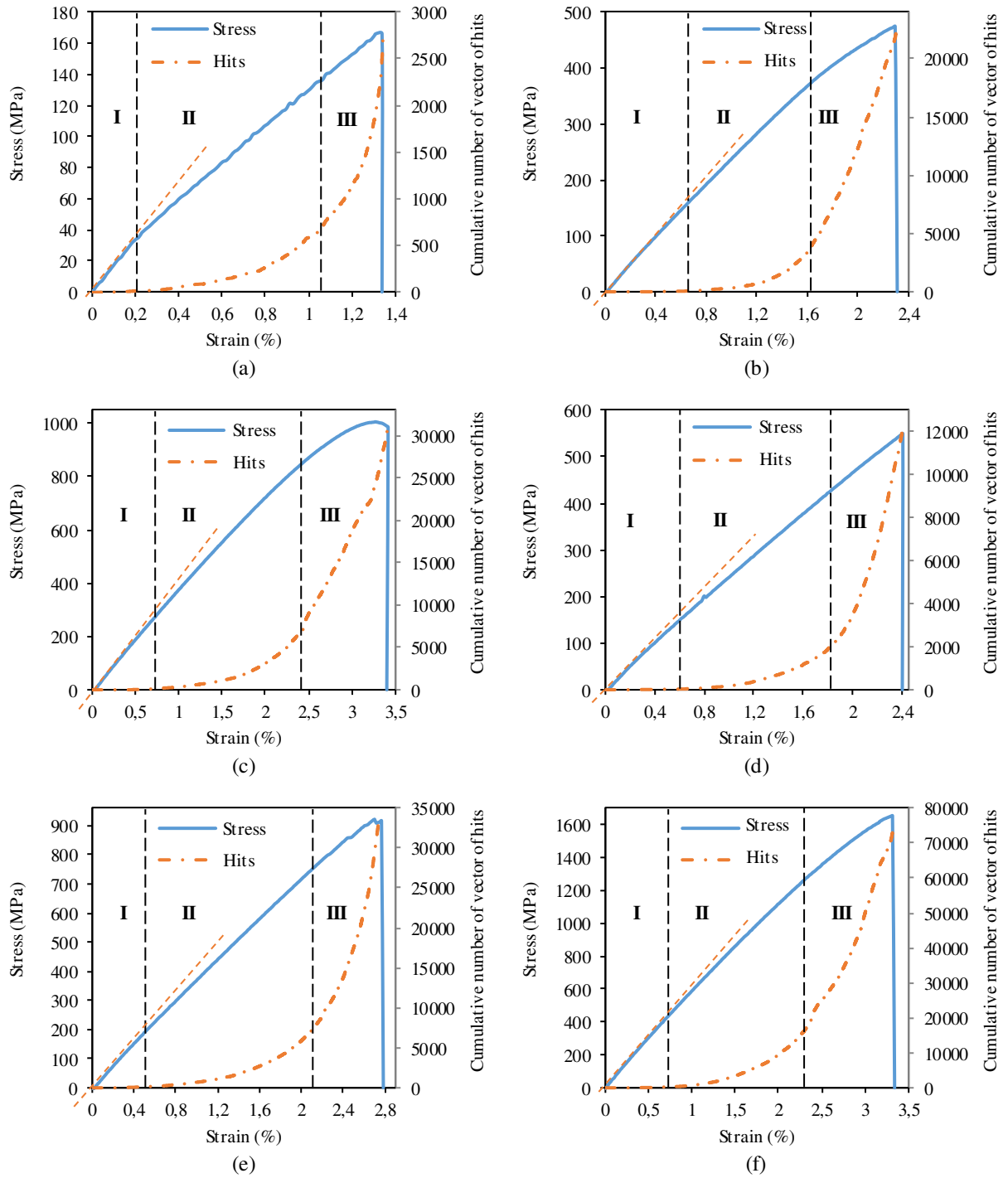


**Fig. 5.** Correlation between the evolution of the acoustic activity and the behavior law for all specimens: a)  $[F_3]_s$ , b)  $[F_2/C]_s$ , c)  $[F/C_2]_s$ , d)  $[C/F_2]_s$ , e)  $[C_2/F]_s$  and f)  $[C_3]_s$ .

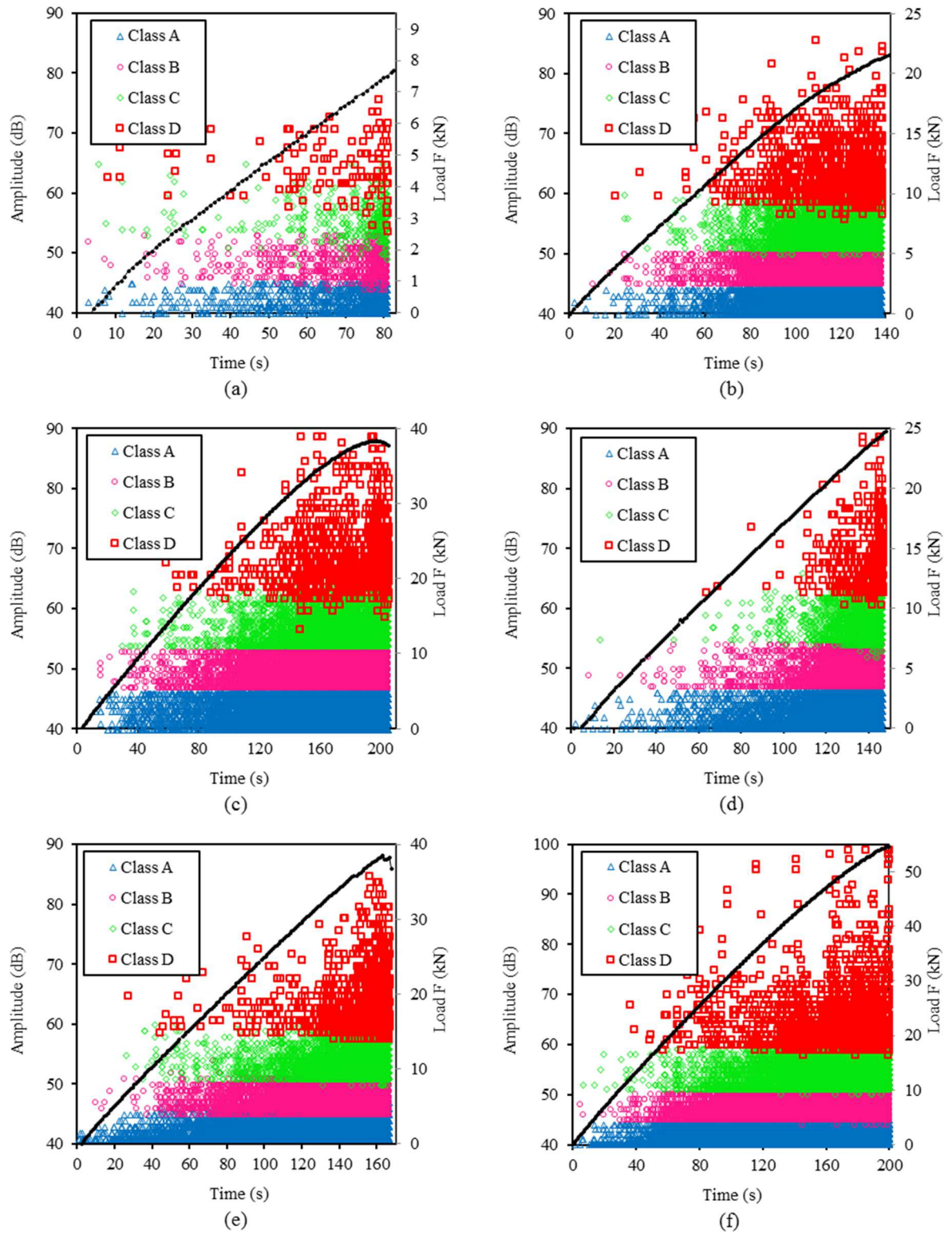
#### 4.2.2. Amplitude Distribution versus time

In order to identify the damage mechanisms occurring in the stacking sequences studied and to pursue their temporal evolution until failure, the clustering methodology based on the five temporal parameters was applied. Fig. 6 shows the distribution of the amplitude of the AE signals versus time during experimental tests, whereas the evolution of the applied load was superposed in the same plot.

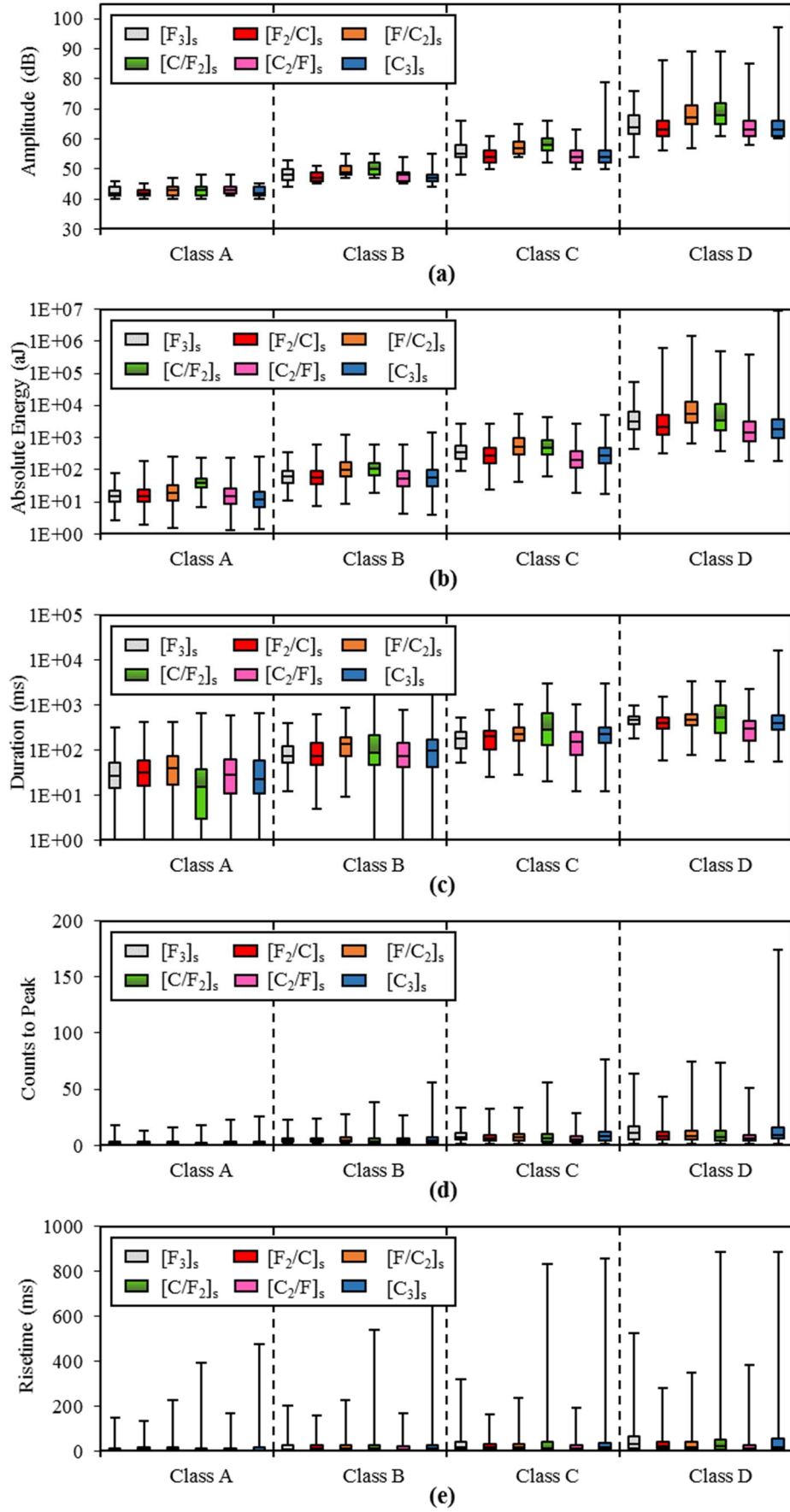
The signal distribution in amplitude shows small areas of intersection between classes for all unidirectional specimens which confirms the application of multi-parameters approach. Four classes were obtained for the non-hybrid ( $[F_3]_s$  and  $[C_3]_s$ ) and hybrid laminates ( $[F_2/C]_s$ ,  $[F/C_2]_s$ ,  $[C/F_2]_s$ , and  $[C_2/F]_s$ ). Only mathematical considerations were used in this classification to constitute the best separation of the AE data, without taking physics into account. According to the literature [12, 13, 53], each class corresponds to a damage mechanism: matrix cracking (class A), fiber-matrix debonding (class B), delamination (class C) and fiber pull-out and fiber breakage (class D). The matrix cracking (class A) is characterized by an amplitude in the range of [40-48 dB]. The second class of signals (class B) induced by fiber/matrix debonding occurs at an amplitude of [44-57 dB]. The class C (delamination mechanism) is characterized by an amplitude between 48 and 65 dB, however, for carbon laminates the amplitude can reach 79 dB. Finally, fiber pull-out and fiber breakage (class D) have an amplitude range of [55-100 dB].

In addition, the attribution of each damage mechanism to the event's class was done using the waveforms of AE signals. Typical forms of the AE waveforms of the four damage mechanisms are given in Table 2.

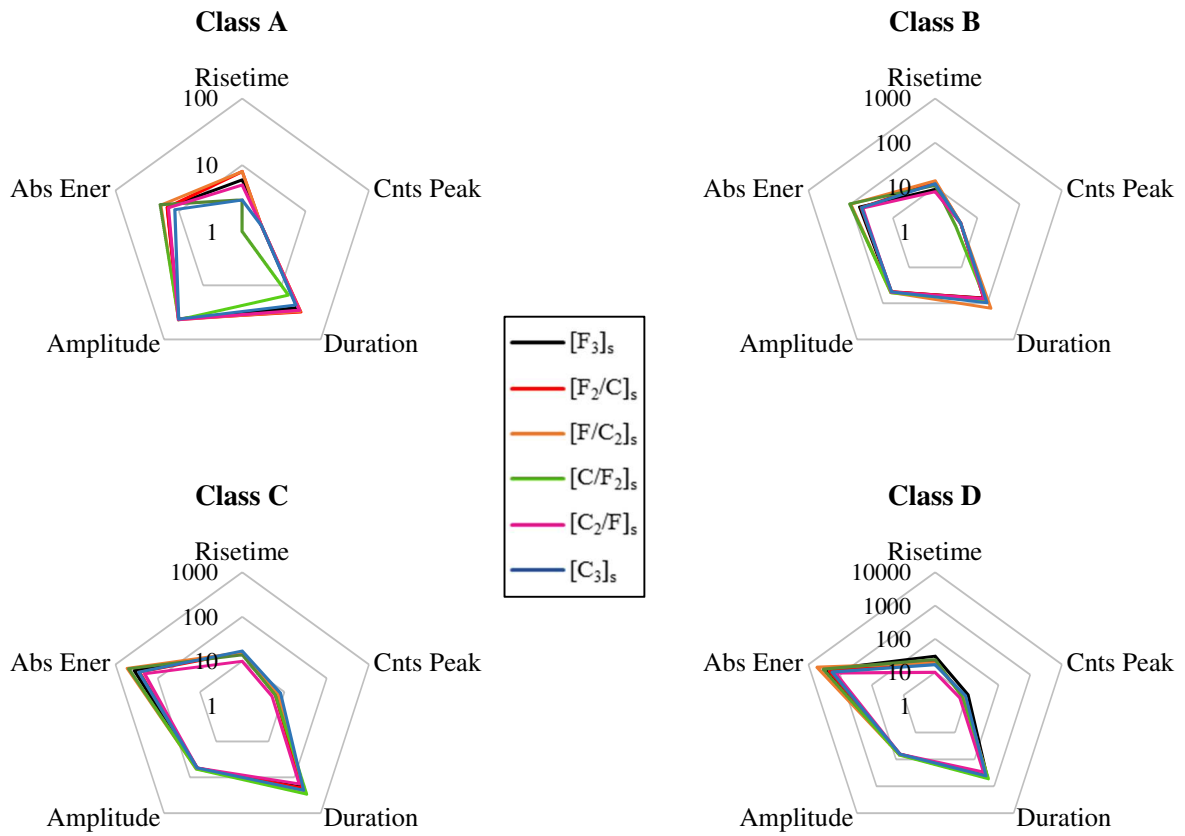
Fig. 7 presents box and whiskers plots for the five classification features with respect to the four AE classes for all laminates. The first quartile  $q_1$  and the third quartile  $q_3$  correspond to the borders of box plots. The second quartile  $q_2$  represents the median corresponding to the line cutting through the box plots. The lower and upper values of the amplitude range of each class correspond to the whiskers in the plot. It is clear that the four classes have quite similar statistical characteristics for the six kinds of specimen. A comparison of the average values of the chosen classification features in the six specimen configurations is shown in Fig. 8. The radar chart clearly shows that the acoustic signatures can be assigned to each class. The average properties for all the specimens are very similar. In fact, according to the average values of descriptors in Fig. 8 and to the typical waveforms in table 2, we can confirm that each damage is characterized by the properties of descriptors. The AE signals induced by the matrix cracking (class A) are characterized by a waveform with low amplitude, slow rise time, relatively long duration and low energy. The second class of signals induced by fiber/matrix debonding (class B) is characterized by low amplitude, short rise time, short duration and low energy. The waveform of the delamination mechanism (class C) is characterized by high amplitude, slow rise time, relatively long duration and low energy. And finally, fiber pull-out and fiber breakage (class D) have a high amplitude, short rise time, very short duration and very great energy.



**Fig. 6.** Distribution of amplitude versus times of AE signals clustering under static tests for all specimens: a)  $[F_3]_s$ , b)  $[F_2/C]_s$ , c)  $[F/C_2]_s$ , d)  $[C/F_2]_s$ , e)  $[C_2/F]_s$  and f)  $[C_3]_s$ .



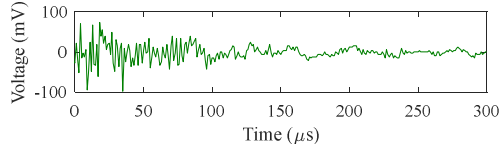
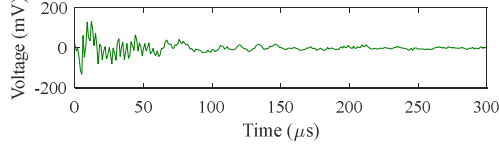
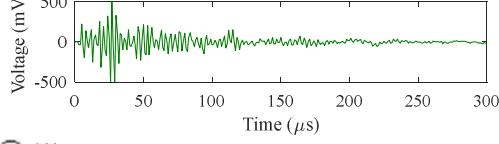
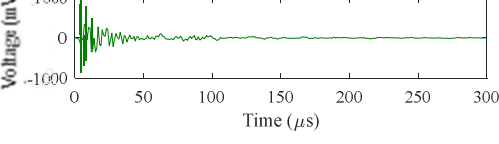
**Fig. 7.** Statistical dispersion of the five classification features versus the four damage mechanisms for non-hybrid and hybrid composites. a) Amplitude, b) absolute energy, c) duration, d) counts to peak and e) risetime.



**Fig. 8.** Average properties of the five classification features with respect to the six kind of specimen for the four damage mechanisms.

**Table 2**

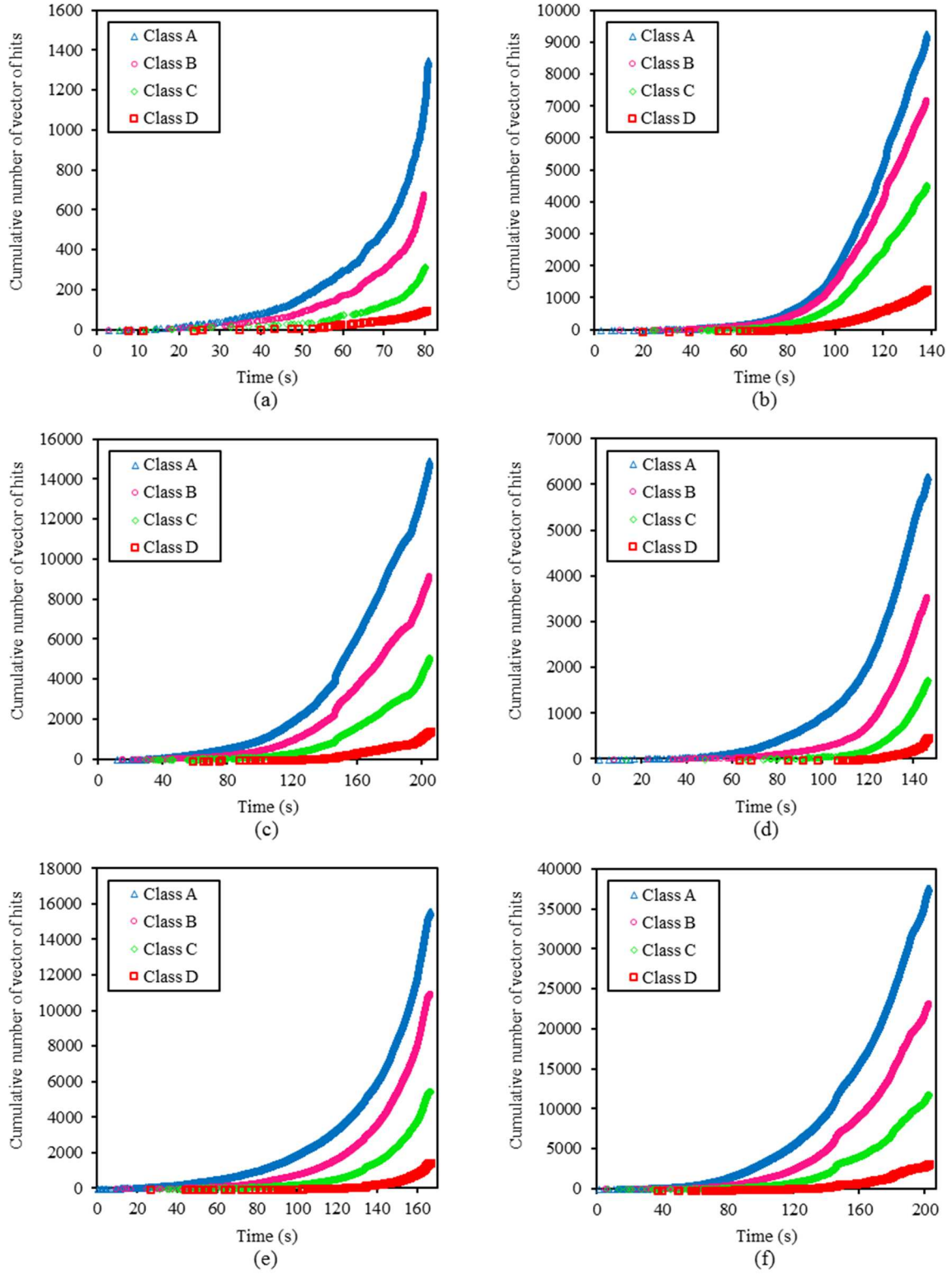
Typical form of AE signals obtained for each damage mechanisms

Damage mechanisms	Form of signal
Matrix cracking (Class A)	
Fiber-matrix debonding (Class B)	
Delamination (Class C)	
Fibers breaking (Class D)	

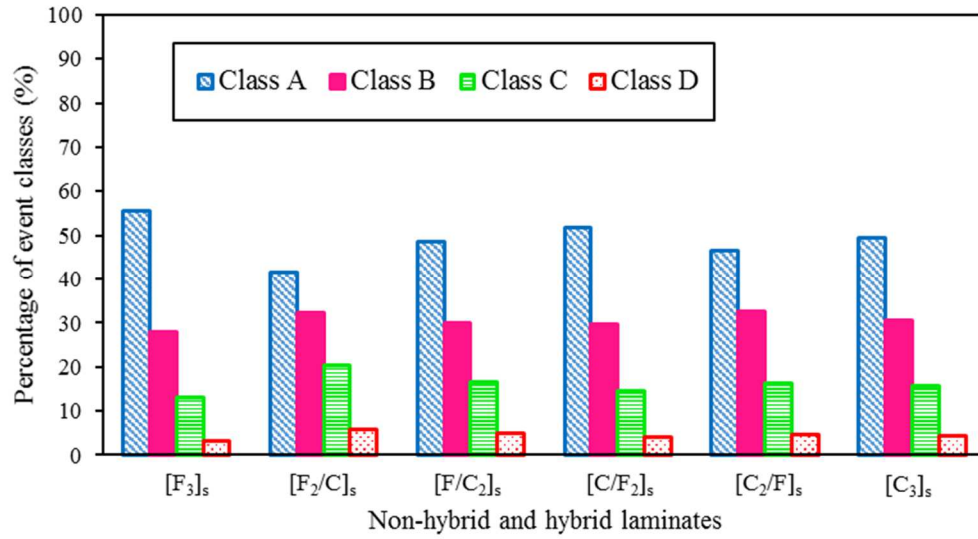
#### 4.2.3. Time dependency of the damage mechanisms identified

Fig. 9 presents the evolution of the cumulative number of vectors of hits for every class as a function of the time. For all specimens studied, the number of hits of every class has a significant increase just before the failure of the specimen. Matrix cracking (class A) is the first damage mechanism appearing in the chronology, and propagates until the specimen's final failure. As shown in Fig. 10, this damage mechanism is the most dominant damage from all types of the specimen and it presents more than 40% of cumulative damage at failure. It is greater for flax fiber laminates than other laminates. This result can be explained by the low fiber volume fraction of flax fibers in the composite structure (fiber volume fraction is 32%). Then, fiber-matrix debonding (class B) appears in the second time after matrix cracking. After that, delamination (class C) and fiber pull-out and fiber breakage (class D) mechanisms occur after around 40% of the breaking load and increase slightly. Fig. 10 also shows that the percentage of fiber breakage, delamination and fiber-matrix debonding for the carbon and hybrid fiber composites is greater than that of flax fiber composites. This is mainly due to the difference in the fiber volume fraction of carbon and flax fiber laminates (0.55 for the carbon fiber laminates vs. 0.32 for the flax fiber laminates). On the other hand, it can be explained by the nature of the adherence between an epoxy resin and carbon fibers compared to the adherence to flax fibers. The radar chart in Fig. 11 presents a comparison between the normalized global vector of hits for the six kinds of the laminates studied for each class. It is clearly seen that when the carbon fiber volume fraction increases the number of vectors of hits increases, for all the AE classes. This fact can be explained by the increasing of rigidity with carbon fibers and then with the increase in applied load. Moreover, the difference between the dimension of carbon fibers and flax fibers may also contribute to these increases (8 $\mu$ m for carbon fiber [54] vs. 15 à 30  $\mu$ m for flax fiber [55]).





**Fig. 9.** Cumulative number of vector of hits under static tests for all specimens: a)  $[F_3]_s$ , b)  $[F_2/C]_s$ , c)  $[F/C_2]_s$ , d)  $[C/F_2]_s$ , e)  $[C_2/F]_s$  and f)  $[C_3]_s$ .



**Fig. 10.** Percentage of cumulative event classes for the studied materials at failure.

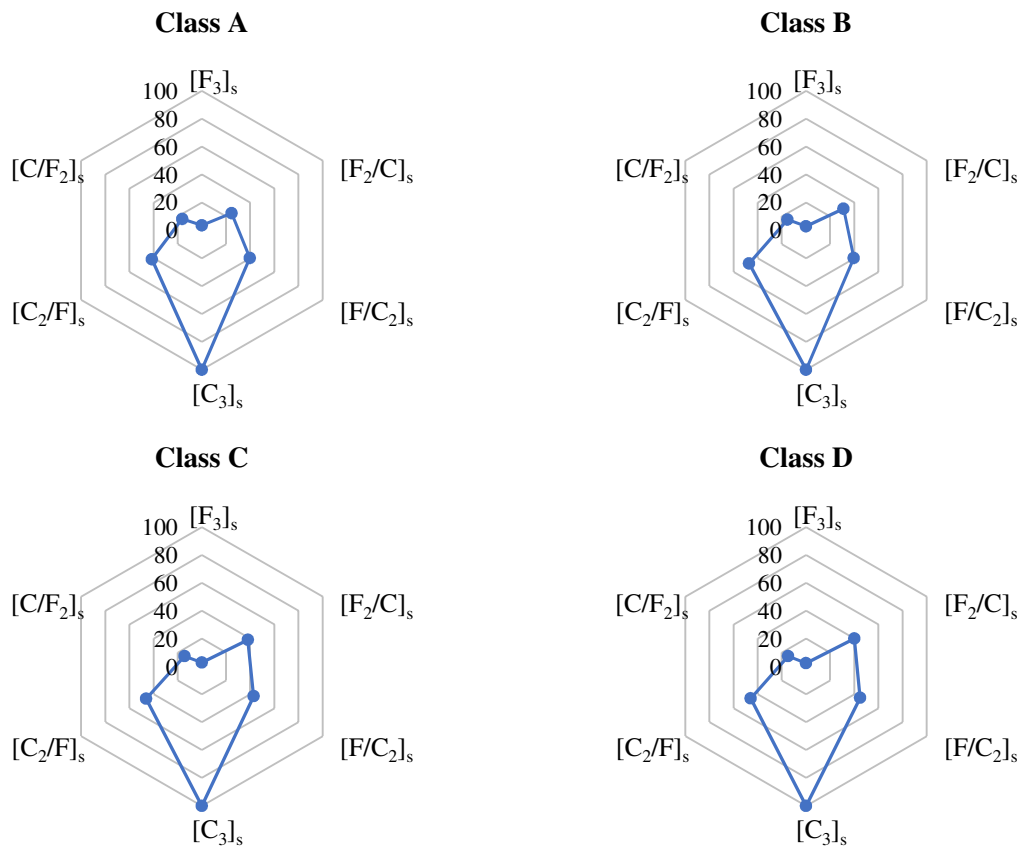


**Fig. 11.** Comparison between normalized global vector of hits for the studied laminates for each class.

#### 4.2.4. Analysis of the contribution of each damage mechanism by the AE energy

The contribution of each damage mechanism to global failure was evaluated for the different stacking sequences. For each damage mechanism, the damage contribution ( $D_i$ ) is obtained by the ratio of the cumulative AE energy of the given mechanism ( $E_i$ ) by the cumulative AE signal energy at failure ( $E_T$ ) [45, 56]:

$$D_i = \frac{E_i}{E_T} = \frac{E_i}{\sum_{j=1}^n E_j} \quad (2)$$

where  $n$  is the total damage mechanism number,  $n = 4$ .

Fig. 12 reports for each damage mechanism the relative contribution  $D_i$  in terms of energy to the final failure for all composite specimens studied. A clear similarity in the  $D_i$  distribution is observed for all types of composites. It is evident that the most significant energy mechanism is the fiber breakage, with more than 72% of the contribution for flax laminates and reaching more than 90% for carbon laminates. The failure of fibers generates a higher absolute energy caused by the great stiffness of fibers. It is evident that the  $D_i$  of the fiber pull-out and fiber breakage in flax fiber laminates (72%) is lower than that of carbon fiber laminates (90%). This fact can be explained by the stiffness of carbon fibers being greater than the stiffness of flax fibers, as it can be explained by the difference in the fiber volume fraction of carbon and flax fiber laminates. This is followed by the contribution of delamination, which is between 10-20% for all composites. And after that, the contribution of fiber-matrix debonding. However, in contrast with fiber pull-out and fiber breakage, the  $D_i$  of delamination and fiber-matrix debonding was the greatest in flax fiber laminates (20% for delamination in flax fiber laminates vs 10% for carbon fiber laminates and 7% for fiber-matrix debonding in flax fiber laminates vs 3% for carbon fiber laminates). As a matter of fact, this difference can be explained by the good adherence between carbon fibers and epoxy resin compared to flax fibers. Finally, although the high cumulative number of vectors of hits for matrix cracking, the contribution of this damage mechanism had very low participation in the energy contribution.

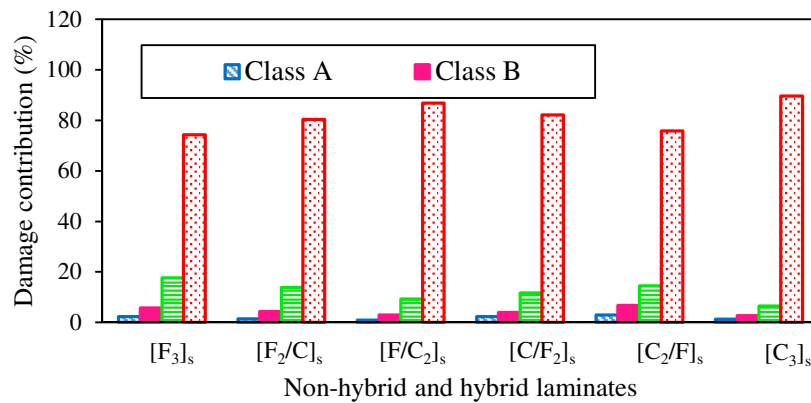


**Fig. 12.** Damage mechanisms contribution for the six studied materials.

### **4.3. Acoustic emission under fatigue tests**

#### **4.3.1. Amplitude distribution versus the number of cycles**

During fatigue tests, the acoustic emission procedure was used to identify the damage mechanism for the different non-hybrid and hybrid laminates. Tests were carried out at a loading ratio of 75% of the ultimate tensile load. Fig. 13 presents the distribution of the amplitude of AE signals according to the number of cycles for all stacking sequences. It reveals the existence of the four classes of damage mechanisms: matrix cracking (class A) with amplitudes from 40-42 dB to 40-45 dB, fiber-matrix debonding (class B) with amplitudes from 42-45 dB to 45-50 dB, delamination (class C) with amplitudes from 45-53 dB to 50-58 dB and fiber pull-out and fiber breakage (class D) with amplitudes from 53 dB up to 100 dB. For the ramp-up period which is before the cyclic period of the fatigue tests, the applied load increases until reaching the mean load imposed. During this period the activity of the AE signals is very low. During the cyclic fatigue test, the distribution of the amplitudes of the collected AE events versus time shows that the AE activity takes place in three phases according to Roundi et al. [52]:

-Phase I: This phase corresponds to the first fatigue cycles. In this phase, we observe the presence of the four damage mechanisms for all the specimens tested. The great damage mechanism corresponds to the initiation and propagation of micro-cracking. The amplitudes of AE events in this phase are between 40 dB and 100 dB.

-Phase II: Followed by the intermediate phase in which AE activity becomes low. This phase involves the propagation of microscopic damage and especially matrix cracking, fiber-matrix debonding and delamination between plies.

-Phase III: Final phase with a high number of AE events followed by specimen failure with the most dominant event being fiber breakage.

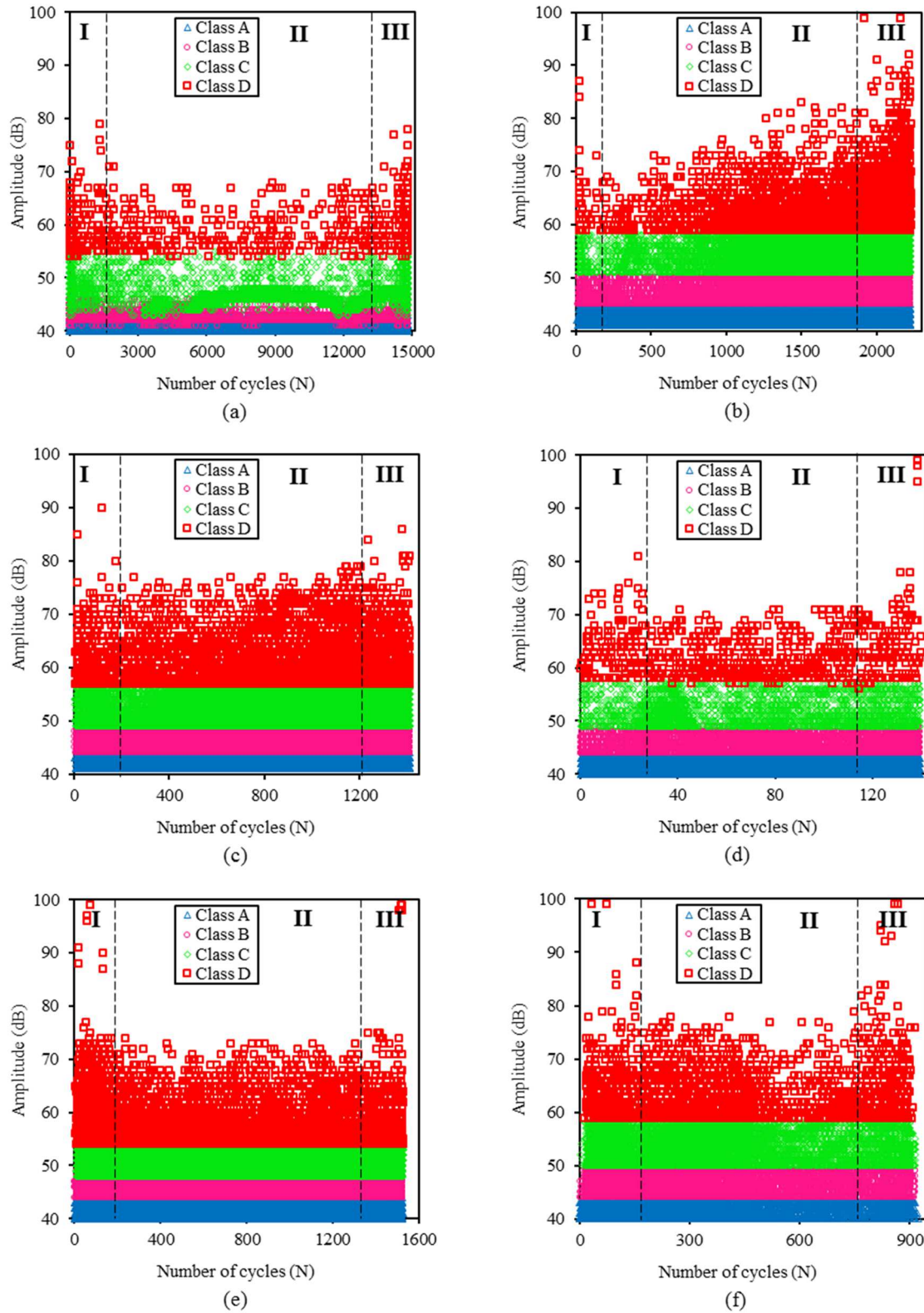


**Fig. 13.** Distribution of amplitude versus times of AE signals clustering under fatigue tests for all specimens:  
a)  $[F_3]_s$ , b)  $[F_2/C]_s$ , c)  $[F/C_2]_s$ , d)  $[C/F_2]_s$ , e)  $[C_2/F]_s$  and f)  $[C_3]_s$ .

#### **4.3.2. Distribution of cumulative number of hits versus the number of cycles**

Matrix cracking events (class A) have the greatest activity for all specimens. Fiber–matrix interface debonding (class B) has less important activity. Delamination (class C) events appear from the start of experimentation and are less numerous than those of class A and class B. This is shown in Fig. 14 which illustrates the evolution of the cumulative number of vector hits versus time for the different stacking sequences, showcasing the different evolution, chronology and amount of the activity events observed throughout the fatigue test. Finally, fiber pull-out and fiber breakage also occur at the beginning of the cyclic period but they are reduced in the intermediate phase and after they increase before final fracture.

Although the relative load level applied is the same for all kinds of specimens, we find that flax fiber laminate composites have a much higher lifetime compared to carbon fiber laminate composites. However, the number of events is greater for carbon fiber laminates in a short lifetime. The results obtained can be due to the low resistance of carbon fiber laminates in reversible loading compared to flax fiber laminates. As a matter of fact, for the hybrid laminates, we find an important number of events in a short lifetime compared to flax fiber laminates. Also, when the flax fiber layers are internal and their volume fraction is higher than those of carbon fiber layers, it is observed that the number of cycles is much lower than hybrid composites with external flax fiber layers. This result can be explained by the fact that active layers are the internal flax layers but the load level applied is imposed in consideration of the carbon layers.

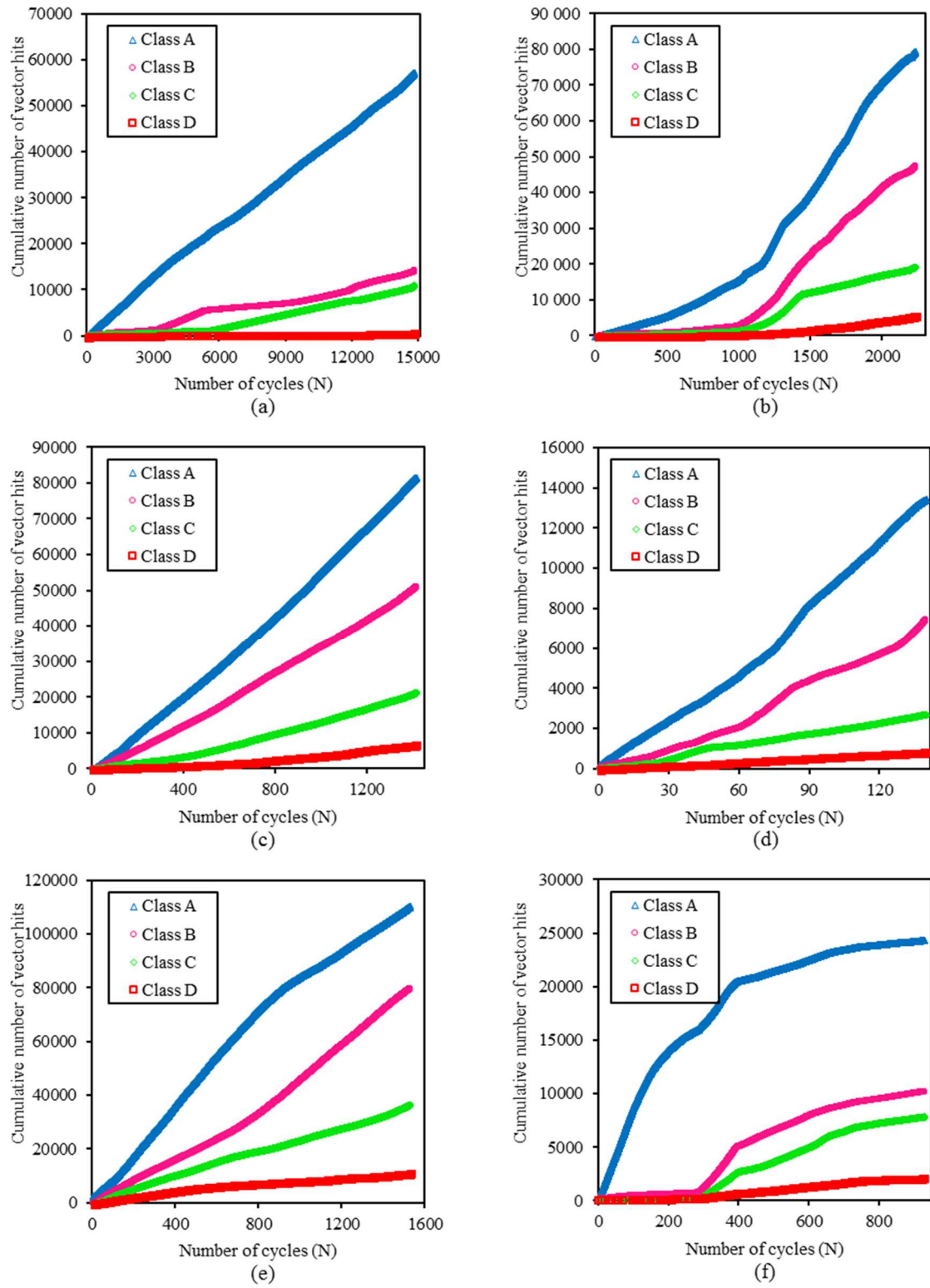


**Fig. 14.** Cumulative number of vector of hits for all specimens under fatigue tests: a)  $[F_3]_s$ , b)  $[F_2/C]_s$ , c)  $[F/C_2]_s$ , d)  $[C/F_2]_s$ , e)  $[C_2/F]_s$  and f)  $[C_3]_s$ .

#### 4.4. Macroscopic and microscopic analyses

To confirm the effectiveness of the multivariable statistical analysis, a correlation with macroscopic and microscopic analyses is carried out. Fig. 15 presents the fractured surface of the six kinds of specimens studied under static tests. At a macroscopic scale, a lot of information can be obtained from these failure profiles. For all these unidirectional specimens, initial cracks a few millimeters long can be detected, followed by propagation of cracks through the tensile axis. Several fibers pull-outs can also be noticed. These failed specimens also exhibit delamination between plies over several millimeters, especially when the carbon fiber volume fraction is higher (Fig. 15c, Fig. 15e and Fig. 15f). In addition, according to the visual inspection of the fractured surface of the materials studied, it is clearly shown that laminates made with carbon fibers present more delamination and fiber breakage in comparison to flax fiber laminates.

Several microscopic analyses were performed by scanning electron microscopy (SEM) of failure profiles and are shown in Fig. 16. The micrographic section of the fractured surface of the flax fiber laminates, for the carbon fiber laminates and for the hybrid fiber laminates are shown in Fig. 16a-c, Fig. 16d-g and Fig. 16h-i, respectively. For the non-hybrid and hybrid specimens, it was quite hard to detect matrix cracking and this was observed in Fig. 16b and Fig. 16e label 1. Generally, it appears to be the propagation of initial cracks at the interface of flax bundles and matrix or carbon fibers and matrix. A lot of unbounded interfaces were observed between adjacent elementary flax fibers inside bundles (Fig. 16c label 3). Fiber-matrix debonding can also be observed for the flax laminates in Fig. 16c label 2 and for the carbon laminates in Fig. 16f label 1. Well-separated flax fibers and carbon fibers were broken very close to the matrix and are observed in Fig. 16b and Fig. 16f label 3. A massive fiber pull-out was observed for every category of specimen (Fig. 16a label 1, Fig. 16g label 1 and Fig. 16i label 2). We can also observe several pulled-out fibers in Fig. 16b label 2 for the flax composite structure and on Fig. 16e and Fig. 16f label 2 for the carbon composite structure. Finally, delamination was also observed in Fig. 16d and Fig. 16h label 1. In addition to the delamination between flax-flax and carbon-carbon fiber layers, a delamination between flax and carbon fiber layers was noticed for the hybrid composites (Fig. 16i label 1).



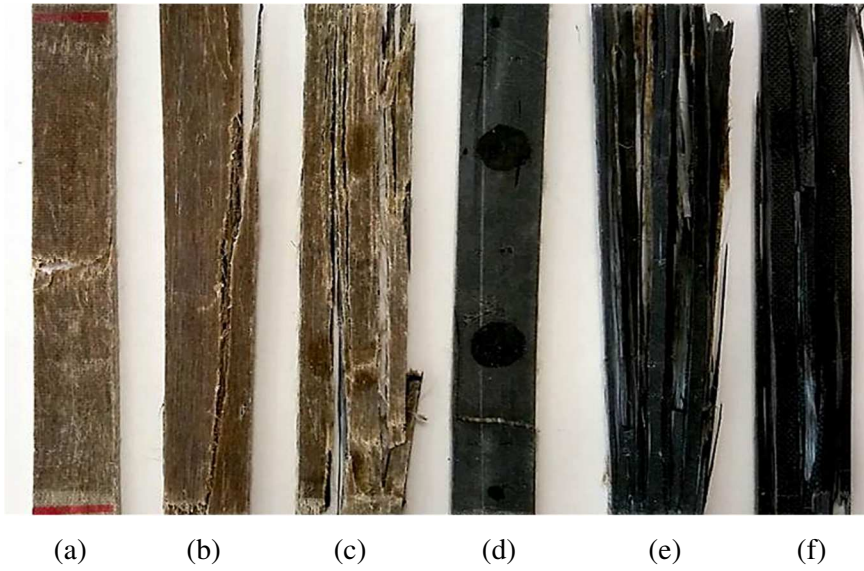


**Fig. 15.** Observation macroscopic of rupture facets in the gauge section for all specimens: a)  $[F_3]_s$ , b)  $[F_2/C]_s$ , c)  $[F/C_2]_s$ , d)  $[C/F_2]_s$ , e)  $[C_2/F]_s$  and f)  $[C_3]_s$ .

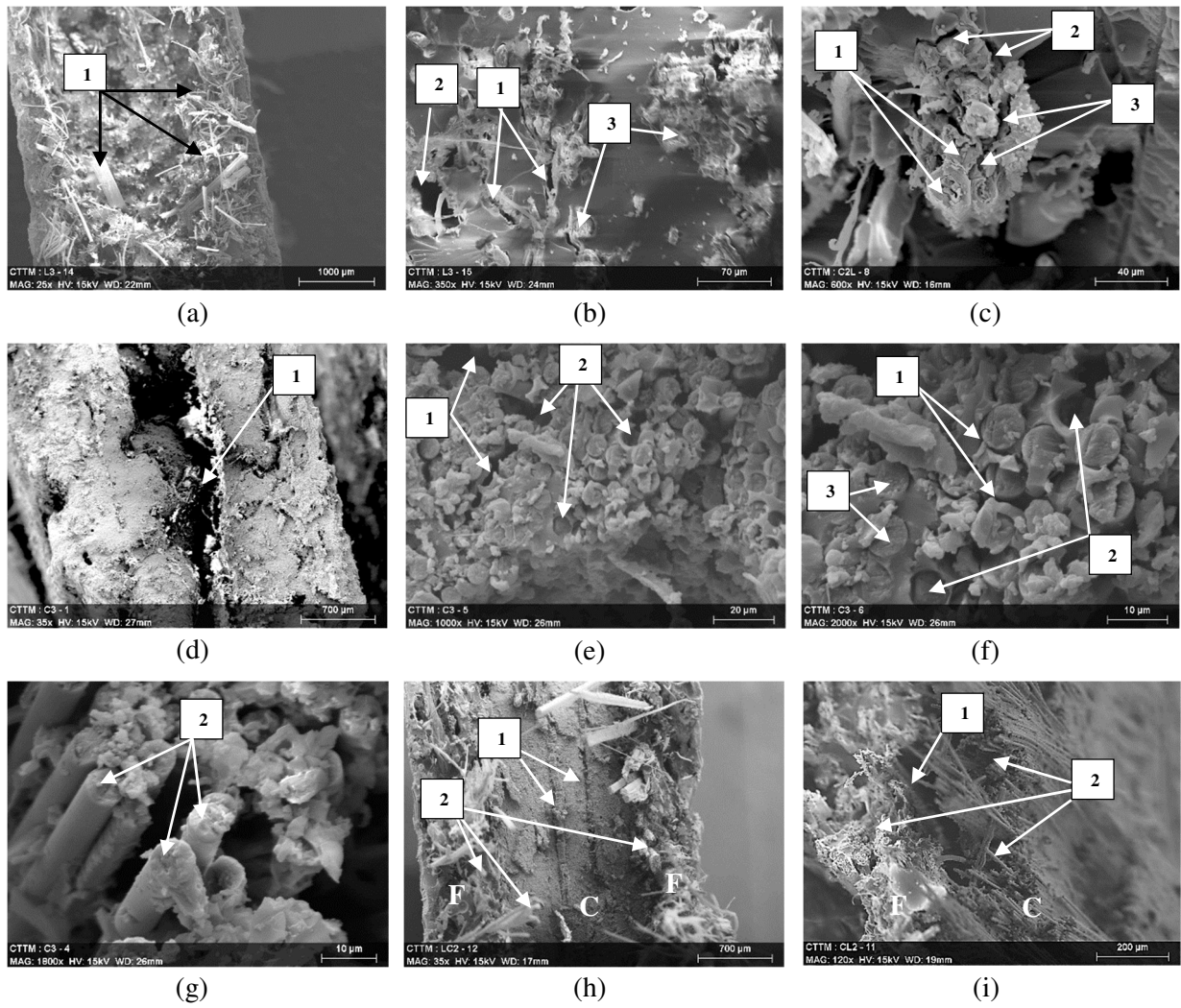


**Fig. 16.** SEM observations of different failure profiles. a)- b)- c) Flax fiber laminates, d)- e)- f)- g) Carbon fiber laminates and h) and i) hybrid fiber laminates.

## 5. Conclusions and perspectives

Monotonic and cyclic fatigue tensile tests were conducted to investigate the evolution of damage mechanisms using the AE technique of hybrid flax-carbon fiber composites. The mechanical results showed that carbon fibers bring about remarkable improvement in the mechanical properties of composites with natural fibers. The multi-variable analyses with five classification features (amplitude, absolute energy, duration, counts to peak and rise-time) were used to classify the AE events. The damage mechanisms were interpreted by using the AE amplitude, vector of hits and the contribution of the AE energy. During static and fatigue tensile testing, the composites studied exhibited four classes of damage mechanisms. Microscopic analyses of the fracture surfaces were carried out in order to correlate the classification obtained from the acoustic events and the damage mechanisms. AE-based damage-mechanism identification revealed that, although the event numbers associated with the fiber breakage were the lowest, their contribution in the cumulative of AE energy to the global failure of composites was the greater. The results obtained reveal that the use of five temporal parameters seems to be sufficient to separate the main groups of events, which have the most noticeable consequences on the mechanical behavior of the composite. However, for flax-carbon hybrid composites, the method used did not allow the identification of AE events related to flax or carbon fibers separately. Therefore, in future work, researchers may use other methods such as the supervised classification method to classify all the AE signals and correlate them with the different damage mechanisms already existing. Finally, in addition to the mechanical properties in the choice of a composite material for a particular application, we should consider the various damage mechanisms and their relative importance, which may be relatively different for different materials and may be crucial for long-term applications.

## References,

- [1] Pickering KL, Efendy MGA, Le TM. A review of recent developments in natural fibre composites and their mechanical performance. *Compos Part Appl Sci Manuf* 2016;83:98–112.
- [2] Faruk O, Bledzki AK, Fink HP, Sain M. Biocomposites reinforced with natural fibers: 2000–2010. *Prog Polym Sci* 2012;37(11):1552–1596.
- [3] AL-Oqla FM, Sapuan SM. Natural fiber reinforced polymer composites in industrial applications: feasibility of date palm fibers for sustainable automotive industry. *J Clean Prod* 2014;66:347–354.
- [4] Wambua P, Ivens J, Verpoest I. Natural fibres: can they replace glass in fibre reinforced plastics? *Compos Sci Technol* 2003;63(9):1259–1264.
- [5] Oksman K. High Quality Flax Fibre Composites Manufactured by the Resin Transfer Moulding Process. *J Reinf Plast Compos* 2001;20(7):621–627.
- [6] Van de Weyenberg I, Ivens J, De Coster A, Kino B, Baetens E, Verpoest I. Influence of processing and chemical treatment of flax fibres on their composites. *Compos Sci Technol* 2003;63(9):1241–1246.
- [7] Hughes M, Carpenter J, Hill C. Deformation and fracture behaviour of flax fibre reinforced thermosetting polymer matrix composites. *J Mater Sci* 2007;42(7):2499–2511.
- [8] Yan L, Chouw N, Jayaraman K. Flax fibre and its composites – A review. *Compos Part B Eng* 2014;56:296–317.
- [9] Sliseris J, Yan L, Kasal B. Numerical modelling of flax short fibre reinforced and flax fibre fabric reinforced polymer composites. *Compos Part B Eng* 2016;89:143–154.
- [10] Monti A, El Mahi A, Jendli Z, Guillaumat L. Experimental and finite elements analysis of the vibration behaviour of a bio-based composite sandwich beam. *Compos Part B Eng* 2017;110:466–475.
- [11] Yan L, Su S, Chouw N. Microstructure, flexural properties and durability of coir fibre reinforced concrete beams externally strengthened with flax FRP composites. *Compos Part B Eng* 2015;80:343–354.
- [12] Monti A, El Mahi A, Jendli Z, Guillaumat L. Mechanical behaviour and damage mechanisms analysis of a flax-fibre reinforced composite by acoustic emission. *Compos Part Appl Sci Manuf* 2016;90:100–110.
- [13] Haggui M, El Mahi A, Jendli Z, Akrouit A, Haddar M. Static and fatigue characterization of flax fiber reinforced thermoplastic composites by acoustic emission. *Appl Acoust* 2018. <https://doi.org/10.1016/j.apacoust.2018.03.011>.
- [14] Duc F, Bourban PE, Plummer CJG, Manson JAE. Damping of thermoset and thermoplastic flax fibre composites. *Compos. Part Appl Sci Manuf* 2014;64:115–123.
- [15] Dhakal HN, Zhang ZY, Guthrie R, MacMullen J, Bennett N. Development of flax/carbon fibre hybrid composites for enhanced properties. *Carbohydr Polym* vol. 2013;96(1):1–8.
- [16] de Moura MFSF, Fernandes R, Silva FGA, Dourado N. Mode II fracture characterization of a hybrid cork/carbon-epoxy laminate. *Compos Part B Eng* 2015;76:44–51.
- [17] Atiqah A, Maleque MA, Jawaaid M, Iqbal M. Development of kenaf-glass reinforced unsaturated polyester hybrid composite for structural applications. *Compos Part B Eng* 2014;56:68–73.
- [18] Ben Ameer M, El Mahi A, Rebiere JL, Abdennadher M, Haddar M. Damping Analysis of Unidirectional Carbon/Flax Fiber Hybrid Composites. *Int J Appl Mech* 2018;10(5):1850050.
- [19] Flynn J, Amiri A, Ulven C. Hybridized carbon and flax fiber composites for tailored performance. *Mater Des* 2016;102:21–29.
- [20] Lemaitre J, Dufailly J. Damage measurements. *Eng Frac Mech* 1987;28(5–6):643–661.
- [21] Todoroki A, Ueda M, Hirano Y. Strain and Damage Monitoring of CFRP Laminates by Means of Electrical Resistance Measurement. *J Solid Mech Mater Eng* 2007;1(8):947–974.
- [22] Chen B, Liu J. Damage in carbon fiber-reinforced concrete, monitored by both electrical resistance measurement and acoustic emission analysis. *Constr Build Mater* 2008;22(11):2196–2201.

- [23] Niccolini G, Borla O, Accornero F, Lacidogna G, Carpinteri A. Scaling in damage by electrical resistance measurements: an application to the terracotta statues of the Sacred Mountain of Varallo Renaissance Complex (Italy). *Rend Lincei* 2015;26(2):203-209.
- [24] Iturrioz I, Lacidogna G, Carpinteri A. Acoustic emission detection in concrete specimens: Experimental analysis and lattice model simulations. *Int J Damage Mech* 2014;23:327-358.
- [25] Rescalvo FJ, Valverde-Palacios I, Suarez E, Roldán A, Gallego A. Monitoring of Carbon Fiber-Reinforced Old Timber Beams via Strain and Multiresonant Acoustic Emission Sensors. *Sensors* 2018;18:1224.
- [26] Dahmene F, Yaacoubi S, et Mountassir ME. Acoustic Emission of Composites Structures: Story, Success, and Challenges. *Phys Procedia* 2015;70:599–603.
- [27] Habibi M, Laperrière L, Lebrun G, Toubal L. Combining short flax fiber mats and unidirectional flax yarns for composite applications: Effect of short flax fibers on biaxial mechanical properties and damage behavior. *Compos Part B Eng* 2017;123:165–178.
- [28] El Mahi A, Ben Salem I, Assarar M, Berbaoui R, Poïlane C, El Guerjouma R. Analyse par émission acoustique de l'endommagement des matériaux éco-composites. 10ème Congrès Français d'Acoustique 2010:7.
- [29] Romhányi G, Karger-Kocsis J, Czirány T. Tensile fracture and failure behavior of technical flax fibers: Technical Flax Fibers. *J Appl Polym Sci* 2003;90(13):3638–3645.
- [30] Bravo A, Toubal L, Koffi D, Erchiqui F. Characterization of Tensile Damage for a Short Birch Fiber-reinforced Polyethylene Composite with Acoustic Emission. *Int J Mater Sci* 2013;3(3):12.
- [31] Aggelis DG, De Sutter S, Verbruggen S, Tsangouri E, Tysmans T. Acoustic Emission Characterization of Damage Sources of Lightweight Hybrid Concrete Beams. *Eng Frac Mech* 2018; doi: <https://doi.org/10.1016/j.engfracmech.2018.04.019>.
- [32] De Groot PJ, Wijnen AM, Janssen RB. Real-time frequency determination of acoustic emission for different fracture mechanisms in Carbon/Epoxy composites. *Compos Sci Technol* 1995;55:405–12.
- [33] Martínez-Jequier J, Gallego A, Suárez E, Juanes FJ, Valea Á. Real-time damage mechanisms assessment in CFRP samples via acoustic emission Lamb wave modal analysis. *Compos Part B-Eng* 2015;68:317–326.
- [34] Stankevych O, Skalsky V. Investigation and identification of fracture types of structural materials by means of acoustic emission analysis. *Eng Frac Mech* 2016;164:24-34.
- [35] Loutas TH, Kostopoulos V, Ramirez-Jimenez C, Pharaoh M. Damage evolution in center-holed glass-polyester composites under quasi-static loading using time-frequency analysis of acoustic emission monitored waveforms, *Composites Science and Technology* 2006;66:1366–1375.
- [36] Qi G. Wavelet-based AE characterization of composite materials, *NDT & E International* 2000;33:133–144.
- [37] Barile C, Casavola C, Pappaletta G. Acoustic emission waveform analysis in CFRP under Mode I test. *Eng Frac Mech* 2018. <https://doi.org/10.1016/j.engfracmech.2018.01.023>.
- [38] Barile C. Innovative mechanical characterization of CFRP by using acoustic emission technique. *Eng Frac Mech* 2018; doi: <https://doi.org/10.1016/j.engfracmech.2018.02.024>.
- [39] Barile C, Casavola C, Pappaletta G, Vimalathithan PK. Acousto-ultrasonic evaluation of interlaminar strength on CFRP laminates. *Compos Struct* 2019 ;208:796-805.
- [40] Gutkin R, Green CJ, Vangrattanachai S, Pinho ST, Robinson P, Curtis PT. On acoustic emission for failure investigation in CFRP: Pattern recognition and peak frequency analyses. *Mech Sys Signal Pr* 2011;25:1393-1407.
- [41] Barile C, Casavola C, Pappaletta G, Vimalathithan PK. Experimental wavelet analysis of acoustic emission signal propagation in CFRP. *Eng Fract Mech* 2018. doi: <https://doi.org/10.1016/j.engfracmech.2018.05.030>.
- [42] Bussiba A, Kupiec M, Piat R, Böhlke T. Fracture characterization of C/C composites under various stress modes by monitoring both mechanical and acoustic responses. *Carbon* 2008;46(4):618–630.
- [43] Bouchak M, Farrow I, Bond I, Rowland C, Menan F. Acoustic emission energy as a fatigue damage

parameter for CFRP composites. *Int J Fatigue* 2007;29(3):457–470.

- [44] Fotouhi M, Suwarta P, Jalalvand M, Czel G, Wisnom MR. Detection of fibre fracture and ply fragmentation in thin-ply UD carbon/glass hybrid laminates using acoustic emission. *Compos Part Appl Sci Manuf* 2016;86:66–76.
- [45] Saidane EH, Scida D, Assarar M, Ayad R. Damage mechanisms assessment of hybrid flax-glass fibre composites using acoustic emission. *Comp Struct* 2017;174:1–11.
- [46] Khalfallah M, Abbès B, Abbès F, Guo YQ, Marcel V, Duval A, Vanfleteren F, Rousseau F. Innovative flax tapes reinforced Acrodur biocomposites: A new alternative for automotive applications. *Mater Des* 2014;64:116–126.
- [47] Baley C, Le Duigou A, Bourmaud A, et Davies P. Influence of drying on the mechanical behaviour of flax fibres and their unidirectional composites. *Compos Part Appl Sci Manuf* 2012;43(8):1226–1233.
- [48] ASTM D30309/D3039M-14: Standard test method for tensile properties of polymer matrix composite.
- [49] Masmoudi S, El Mahi A, Turki S. Fatigue behaviour and structural health monitoring by acoustic emission of E-glass/epoxy laminates with piezoelectric implant. *Appl Acoust* 2016;108:50–58.
- [50] Nielsen A. Acoustic emission source based on pencil lead breaking. Danish Welding Institute Publication; 1980;80:15.
- [51] Kattis S. Noesis - Advanced Data Analysis, Pattern Recognition & Neural Networks Software for Acoustic Emission Applications. p. 8.
- [52] Likas A, Vlassis N, Verbeek JJ. The global k-means clustering algorithm. *Pattern Recognit* 2003;36(2):451–461.
- [53] Roundi W, El Mahi A, El Gharad A, Rebiere JL. Acoustic emission monitoring of damage progression in Glass/Epoxy composites during static and fatigue tensile tests. *Appl Acoust* 2018;132:124–134.
- [54] Ben Ammar I. Contrôle de santé vibro-acoustique de l'endommagement des matériaux composites à base polymère pour l'aéronautique. PhD dissertation, Le Mans Université, France, 2014.
- [55] Monti A. Elaboration et caractérisation mécanique d'une structure composite sandwich à base de constituants naturels. PhD dissertation, Le Mans Université, France, 2016.
- [56] Bravo A, Toubal L, Koffi D, Erchiqui F. Development of novel green and biocomposite materials: Tensile and flexural properties and damage analysis using acoustic emission. *Mater Des* 2015;66:16–28.